JOURNAL OF MATERIALS SCIENCE: MATERIALS IN MEDICINE 5 (1994) 533–542

Densification and strengthening of silver-reinforced hydroxyapatite-matrix composite prepared by sintering

T. K. CHAKI, P. E. WANG
Department of Mechanical and Aerospace Engineering, State University of New York, Buffalo, NY 14260-4400, USA

Ductile-phase reinforcement of hydroxyapatite (HA) was achieved by addition of silver particulates (5–30 vol%) in HA powder and subsequent sintering of HA–Ag powder compacts. A composite made by sintering 10 vol% Ag and the balance HA at 1200 °C for 1 h in air had flexural strength of 75 ± 7 MPa, which was almost double that of pure HA sintered under an identical condition. The density of HA-10 vol% Ag composite was 90 ± 2% of the theoretical density (as calculated from the rule of mixture) and was lower than that (98.7 ± 0.4%) of pure HA sintered at a similar condition. The X-ray diffraction pattern of the composite did not indicate any decomposition of HA or any reaction between HA and Ag. Ag in the composite melted during sintering, but, due to poor wetting, did not spread in between HA particles. The addition of Ag reduced densification and grain growth during sintering of HA–Ag composites. Indentation cracks in the composites went around Ag inclusions and often stopped at Ag inclusions. The increase in the flexural strength of the composites was thought to be due to crack-bridging and crack-arrest by silver particles.

1. Introduction

Over the last several years calcium phosphate compounds [1] have been studied for use as biomaterials [2, 3] in bone implantation. The major constituent [4] of bone is hydroxyapatite (abbreviated as HA) and its chemical formula is $Ca_{10}(PO_4)_6(OH)_2$. It crystallizes into hexagonal structure [5] with unit cell dimensions of $a = 0.9432$ nm and $c = 0.6881$ nm. Its theoretical density is 3.08 g cm^{-3}, lighter than metallic implants (the densities of titanium, stainless steel and cast stellite are 4.5, 7.9 and 8.3 g cm^{-3}, respectively). Defective HA can, however, occur with the Ca/P ratio deviated from $10/6 = 1.67$. The most interesting property of HA is its excellent biocompatibility [6–8]. Tissue can infiltrate HA and also form chemical bonding with HA.

HA is a ceramic material. Its powder can be formed into blocks with various densities and strengths by pressureless sintering, hot pressing and hot isostatic pressing [9]. Winter *et al.* [10] suggested a correspondence between compactness of calcium phosphate implants and physiological acceptance. Studies of porous HA implants on dogs' alveolar ridges [11] and human maxillary alveolus [12] demonstrated bone ingrowth into the open pores on the surface of the implants. On the other hand, studies in dogs [13, 14] and biopsy specimens from humans [15, 16] showed that dense HA implants became surrounded by mature fibrous tissue, with a variable amount of new bone formation. However, HA implants often developed cracks [10, 14]. In fact, brittleness of HA is a serious obstacle to its use as load-bearing implants. Recently, Wang and Chaki [17] have shown that decomposition of HA hinders sintering and degrades mechanical properties. They have concluded that in air the maximum sintering temperature should not be above 1200 °C and in vacuum it should not be above 1000 °C.

Several efforts have been made to prepare biomaterials by mixing HA with other materials. Such composites are intended to have higher strength and fracture toughness than monolithic HA. Resorbable binders, such as plaster of Paris, have been used [18] after filling with HA particles. Upon implantation, the binder is gradually resorbed and infiltration of tissue occurs, maintaining the integrity of the implant. Another composite which has earned popularity is HA-filled polyethylene [19]. The polyethylene-matrix composites with various volume fractions of HA between 40 and 60% can simulate elastic modulii of bone. Acrylic bone cement containing HA as a filler has been developed [20], with an addition of 4-methacryloyloxyethyl trimellitate anhydride (5 wt%) to promote adhesion to bone. An HA-filled poly(L-lactide) composite [21] containing 30 wt% HA had improved compressive and tensile strengths, stiffness and hardness. One drawback of the above-mentioned composites [18–21] is that most HA particles are surrounded by the binder or the polymer such that, when the composite is implanted, the tissue does not come into direct contact with HA particles.

A few composites have been developed by sintering mixtures of powders of HA and another ceramic. Ji and Marquis [22] prepared a composite by sintering a

mixture of HA and 20 wt % Al_2O_3 powders at 1400 °C for 2–4 h. Bertoluzza *et al.* [23] prepared a similar HA/Al_2O_3 composite by sintering at 1200 °C for 1 h. The composite showed good biocompatibility with bone growth [23] into it. However, Al_2O_3 interacts with HA, forming calcium aluminate [22, 23].

Ceramic-matrix metal composites (known as cermet [24]) containing small amounts (20–30 vol %) of a ductile metal are known to have higher fracture toughness than the monolithic ceramic. In such composites the strength of the ceramic is maintained while brittleness is avoided by interception of the cracks by ductile metal particles, by crack-bridging [25] at unbroken ligaments of metal particles in the wake of the crack tip and by plastic deformation of the metallic phase. The examples of a few successful cermets are Al_2O_3 reinforced by Al [26], WC reinforced by Co [27] and $MoSi_2$ reinforced by Nb [28]. Cermets of HA and a metal can be prepared by powder metallurgical techniques. If the metal is biocompatible, the cermet of HA should have excellent biocompatibility, high strength and improved toughness. Rogier and Pernot [29] prepared a composite of calcium alumino phosphate glass and titanium (3.5–50 vol %) by vacuum hot pressing at 700 °C and suggested that microcracks generated due to thermal and elastic mismatches between HA and Ti deteriorated mechanical properties.

The objective of the present study is to prepare HA-matrix composites reinforced by silver particles and to investigate their microstructures and mechanical properties. In addition to acting as the reinforcing agent, Ag can have antibacterial effectiveness [30]. Furthermore, HA–Ag composites can be prepared by sintering in air, without causing any oxidation to Ag. Silver, being a noble metal, is quite inert and corrosion-resistant.

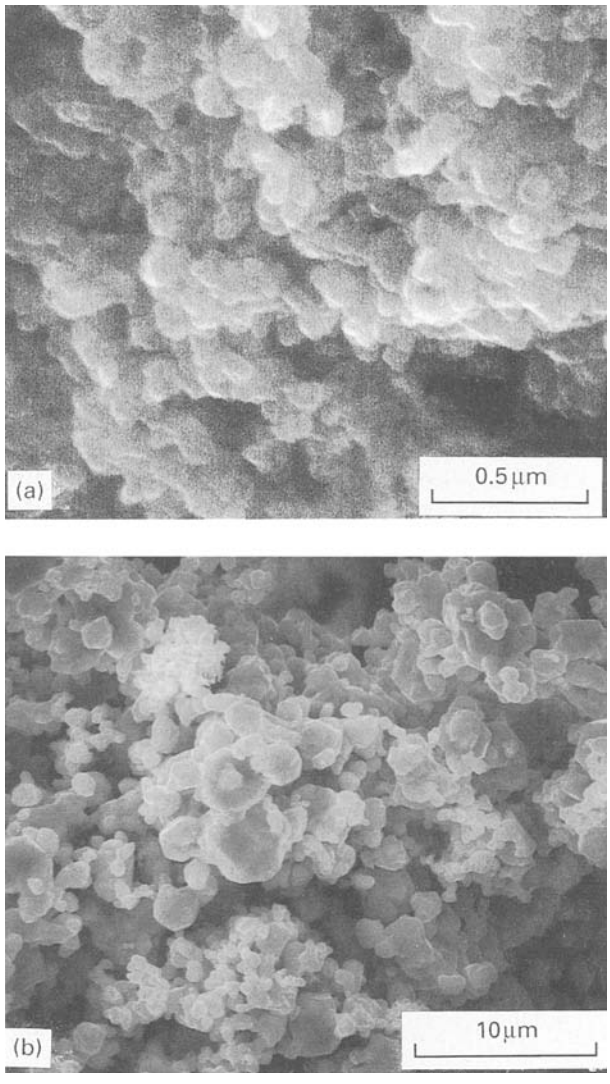

Figure 1 Scanning electron micrographs of HA particles (a) and Ag particles (b).

2. Materials and methods

HA powder was purchased under the name calcium phosphate tribasic from E.M. Science (Associate of E. Merck, Darmstadt, Germany). The impurity contents (as reported by the vendor) by weight were: chloride < 0.1%, fluoride < 0.005%, sulphate < 0.5%; As < 2 ppm, heavy metals (such as Pb) < 0.003%, Fe < 0.04% and H_2O < 2.5%. The particles in HA powder are quite fine, with specific surface area (measured by BET technique) 62.4 $m^2 g^{-1}$. The shape of HA particles was nearly round, as shown in the micrograph (Fig. 1a) taken with the help of a field emission scanning electron microscope (Hitachi S-800) at a magnification of 50 000 ×. To avoid charging during SEM work, HA particles were coated by arc discharge with carbon film of approximate thickness of 10 nm. As a result of coating, the particles in Fig. 1a appear larger than the actual size. That the purchased calcium phosphate was really HA was checked by measuring the Ca/P ratio and analysing the powder X-ray diffraction pattern. The Ca/P atomic ratio was measured by chemical analysis. HA powder was dissolved in 50% concentrated HCl and the concentration of Ca ions in the solution was measured by atomic absorption spectrometer. The concentration of PO_4 ions was determined from the ultraviolet absorption spectrum of a molybdivanadophosphate complex [31]. HA powder was examined in a Nicolet X-ray diffractometer with CuK_α radiation. The diffraction patterns were compared with the database in American Society for Testing and Materials powder diffraction files. Silver powder (99.9% pure) was purchased from Johnson Matthey Co. The specific surface area of Ag particles was 0.75 $m^2 g^{-1}$. The particles were nearly round, as shown in Fig. 1b. 90% of the Ag particles had a size in the range 1–3 μm (measured with the help of a particle analyser).

The HA and Ag (5–30 vol % Ag) powders were mixed by ball-milling in an alumina-coated porcelain jar for about 10 min. The mixture was poured into a bowl and again mixed manually with a spoon for about 2 min to undo any separation of Ag particles during pouring. Pure HA powder and the composite powder were compacted at room temperature inside steel dies under a uniaxial stress of 350 MPa. For lubrication the interior surfaces of the die were coated by applying a layer of stearic acid with a brush and then drying. The green compacts were prepared in

rectangular shapes of two sizes, namely 14 mm × 7 mm × 6 mm and 48 mm × 7 mm × 5 mm. The green compacts were sintered in air for up to 4 h in the temperature range 900–1300 °C. After sintering, in all cases the specimens were slowly cooled inside the furnace, typically at a rate of 100 °C h^{-1}.

To determine densification due to sintering, 14-mm-long specimens were ground by emery papers to precise rectangular shape (within 0.05 mm). To avoid absorption of water during density measurement, the grinding was done in dry conditions. The volume of the rectangular block was calculated from the dimensions measured with the help of a slide caliper and its weight was measured by a balance. Since HA–Ag composites prepared by sintering contain pores, density was expressed in terms of relative density, which is the ratio of the actual density and the theoretical density. The rule of mixture was used to calculate the theoretical density (ρ_{th}) of the composites:

$$\rho_{th} = V_{HA}\rho_{HA} + V_{Ag}\rho_{Ag} \quad (1)$$

where V_{HA}, V_{Ag} are the volume fractions of HA and Ag, respectively and ρ_{HA}, ρ_{Ag} are the densities of HA and Ag, respectively. Since the relative green densities (the density before sintering) of the as-pressed composites with various Ag contents were different, the densification due to sintering was expressed in terms of a quantity called densification factor [32], which provides a measure of pore elimination due to sintering. The densification factor (DF) was calculated using the following formula:

$$DF = (\rho_t - \rho_g)/(\rho_{th} - \rho_g) \quad (2)$$

where ρ_t, ρ_g and ρ_{th} are the density upon sintering for a time t, the green density and the theoretical density, respectively.

The surface of some of the blocks was polished with alumina slurry up to 0.1 μm. Hardness was measured by Knoop indentation on the shiny surface. The load applied during Knoop indentation was 200 g. The Knoop hardness (KHN) was calculated using the formula:

$$KHN = \frac{P}{cl^2} \quad (3)$$

where P is the load, l is the diagonal (longer) length of the indentation and c is a constant, whose value was taken as 0.07028,. The sintered bars (48 mm long) were used for measuring flexural strength. Four-point bending tests were performed on the sintered bars following US military standard [33]. The distance between the outer rollers was 40 mm. The flexural strength (σ) was calculated by the formula:

$$\sigma = \frac{3PL}{4bd^2} \quad (4)$$

where P is the load at which the specimen breaks, L is the distance between the outer rollers, b is the width of the specimen and d is the thickness of the specimen.

For metallographic examinations, a few of the small rectangular blocks was cut in cross-section. The cross-section was ground with emery paper and polished with alumina slurry up to 0.1 μm. To reveal the grain structure, the polished cross-section was etched with 85% concentrated lactic acid for several minutes. The etched surface was examined by optical microscopy. The grain size was measured by the intercept method [34] from the optical micrographs. The fracture surfaces of a few specimens broken by four-point bending were examined by scanning electron microscope. Indentation cracks were generated on the polished surface of the composite specimen by Vickers indenter. The propagation of the cracks around Ag particles was examined with the help of an optical microscope.

3. Results and discussion

3.1. Densification

The sintering temperature had a significant influence on the densification of HA–Ag composites. The densities of both pure HA and HA–Ag composites increased rapidly with the sintering temperature to 1200 °C and then started to decrease. Fig. 2 shows plots of density against sintering temperature for HA-10 vol % Ag composite and pure HA. At each temperature, sintering was done for 4 h in air. Each datum point in Fig. 2 was averaged over measurements on at least three specimens. The typical error in the density measurement was about 2%. Note that the relative green density of HA-10 vol % Ag composite was slightly higher than that of pure HA, both materials being compacted under a uniaxial stress of 350 MPa.

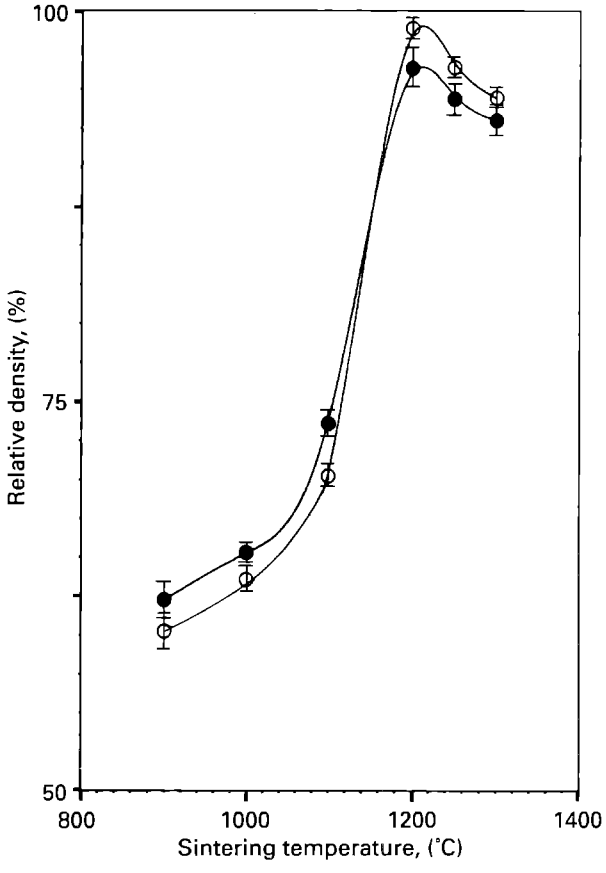

Figure 2 Densities of pure HA and HA-10 vol % Ag composite against the sintering temperature. The open and solid circles correspond to pure HA and HA–Ag composite, respectively. At each temperature sintering was for 4 h in air.

TABLE I Density (ρ_t, g cm^{-3}) and densification factor (DF) after sintering in air at 1200 °C

		Pure HA	5 o/v Ag	10 o/v Ag	15 o/v Ag	20 o/v Ag	30 o/v Ag
Theoretical density (g cm^{-3})		3.08	3.45	3.82	4.19	4.56	5.31
Green density (g cm^{-3})		1.63	1.88	2.19	2.39	2.64	3.11
5 min	ρ_t	2.01	2.18	2.39	2.50	2.74	3.23
	DF	0.262	0.191	0.123	0.061	0.052	0.054
10 min	ρ_t	2.75	2.91	3.21	3.35	3.60	4.07
	DF	0.770	0.656	0.626	0.533	0.500	0.436
20 min	ρ_t	2.86	3.12	3.29	3.62	3.88	4.15
	DF	0.848	0.790	0.675	0.683	0.646	0.473
30 min	ρ_t	3.01	3.23	3.33	3.65	3.91	4.36
	DF	0.952	0.860	0.699	0.700	0.661	0.568
60 min	ρ_t	3.04	3.30	3.43	3.67	3.96	4.44
	DF	0.972	0.904	0.761	0.711	0.687	0.604
120 min	ρ_t	3.04	3.32	3.68	3.72	4.00	4.55
	DF	0.972	0.917	0.914	0.739	0.708	0.655
240 min	ρ_t	3.04	3.36	3.68	3.88	4.21	4.84
	DF	0.972	0.943	0.914	0.828	0.818	0.786

The higher relative green densities of the composites are due to better packing [35] of the mixture of HA and Ag particles with different sizes and due to plastic deformation of Ag particles under compaction. The theoretical and green densities (in g cm^{-3}) of the composites containing various volume fractions of Ag are shown in Table I.

In a previous paper [17] it was shown that sintering of HA is affected adversely by decomposition of HA at temperatures above 1200 °C in air. The decomposition decreased (Fig. 2) the densities of pure HA and composites at sintering temperatures above 1200 °C. Another interesting point to note in Fig. 2 is that, even though the relative green density of HA-10 vol % Ag composite was higher than that of pure HA, the maximum relative density of the composite, obtained upon sintering at 1200 °C for 4 h was 93%, which was lower than the relative density (99%) of pure HA at the corresponding sintering condition. The relative density of the composite remained lower than that of pure HA at sintering temperatures higher than 1200 °C. Ag melted at sintering temperatures above 960 °C, but did not contribute to the shrinkage of HA. The reason for this will be discussed in the section on microstructure. That the addition of Ag did not help sintering of HA is demonstrated further in Fig. 3, where the relative densities of the composites were plotted against the volume fraction of Ag. The composites with various Ag contents were prepared by sintering at 1200 °C in air for 1 h. The relative density of the composite decreased with increasing Ag content.

Another phenomenon which could affect sintering is that droplets of Ag sweated out of the surface of the specimens during sintering. Fig. 4 shows photographs of blocks of pure HA and composites containing 5, 10, 15, 20 and 30 vol % Ag after sintering at 1200 °C in air for 4 h. Molten Ag flowed and sometimes collected (seen as white spots in Fig. 4) near the surface, and some shiny droplets pierced out of the surface. Similar sweating of Ag has been reported [36] in an

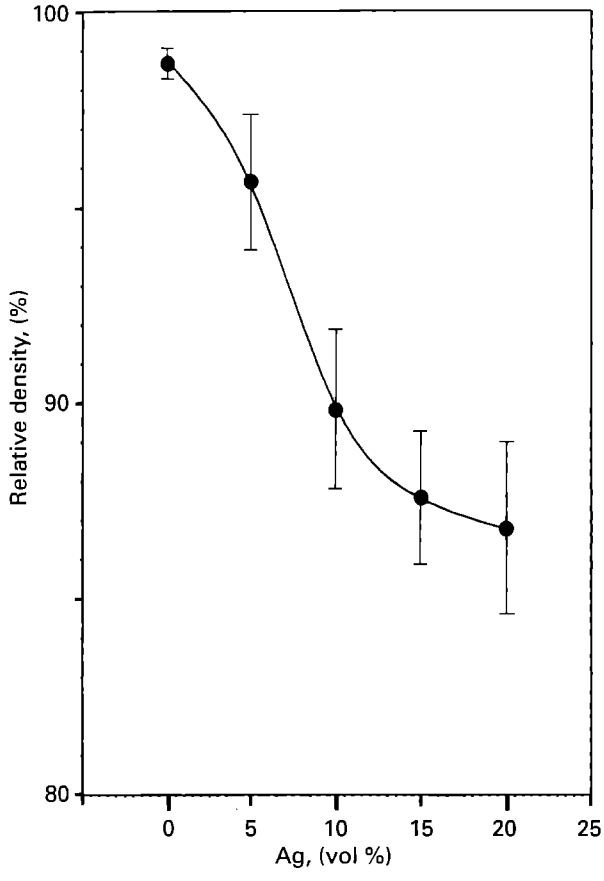

Figure 3 Density against Ag content of the composites after sintering at 1200 °C in air for 1 h.

Al_2O_3–Ag system sintered in air at 1000–1250 °C. Fig. 4 shows that the size of the droplets became larger as Ag content in the composites was increased. It should be noted that, if there is loss of Ag due to sweating, our calculated relative density would be lower than the actual relative density, because the theoretical density of the composite was calculated from the nominal composition using the rule of mixture. In composites containing 5 and 10 vol % Ag the weight loss due to sweating of Ag was small (much less than 1%), but the

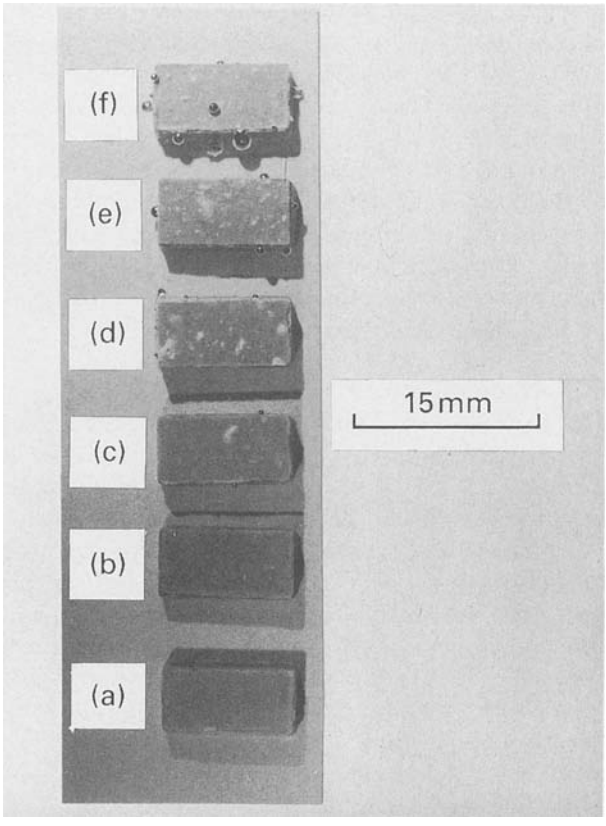

Figure 4 Sweating of Ag droplets in composites sintered at 1200 °C in air for 4 h. Specimen (a) corresponds to pure HA. Specimens (b), (c), (d), (e) and (f) correspond to composites containing 5, 10, 15, 20 and 30 vol % of Ag, respectively.

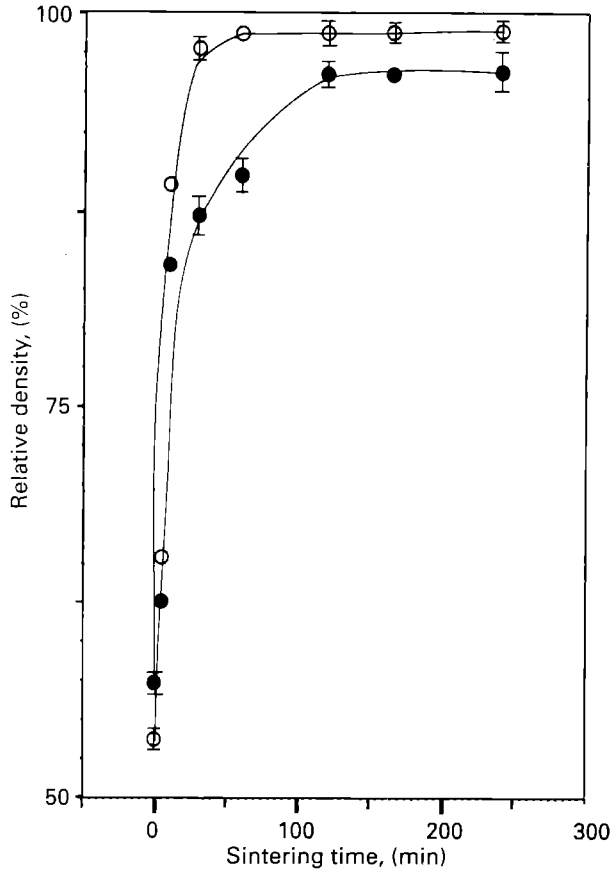

Figure 5 The relative densities of pure HA (○) and HA-10 vol % Ag composite (●) against sintering time at 1200 °C.

relative density decreased rapidly (Fig. 3) as the volume fraction of Ag was increased from 0 to 10%.

The density of HA–Ag composite increased rapidly at the initial stage of sintering, but eventually reached a plateau. Fig. 5 shows the relative density of HA-10 vol % Ag composite against time during sintering in air at 1200 °C. For comparison, the relative density of pure HA was also plotted against sintering time in Fig. 5. The relative density of HA-10 vol % Ag composite reached a saturation value (96%) after 2 h sintering at 1200 °C, while that of pure HA reached a higher value (99%) in only 1 h. Table I shows the absolute densities (in g cm^{-3}) and densification factors of the composites containing 5–30 vol % Ag upon sintering at 1200 °C for various time periods in the range 5–240 min. At an identical sintering condition the absolute density increased with increasing Ag content, but the densification factor decreased, indicating that the shrinkage achieved by sintering was less at higher Ag contents. Fig. 6 shows the evolution of densification factor of HA–Ag composites containing 5–30 vol % of Ag upon sintering in air at 1200 °C. For all volume fractions of Ag, the densification factor initially increased rapidly and eventually reached plateaus. After 240 min sintering at 1200 °C, the densification factor decreased with Ag content from 0.972 for pure HA to 0.786 for 30 vol% Ag.

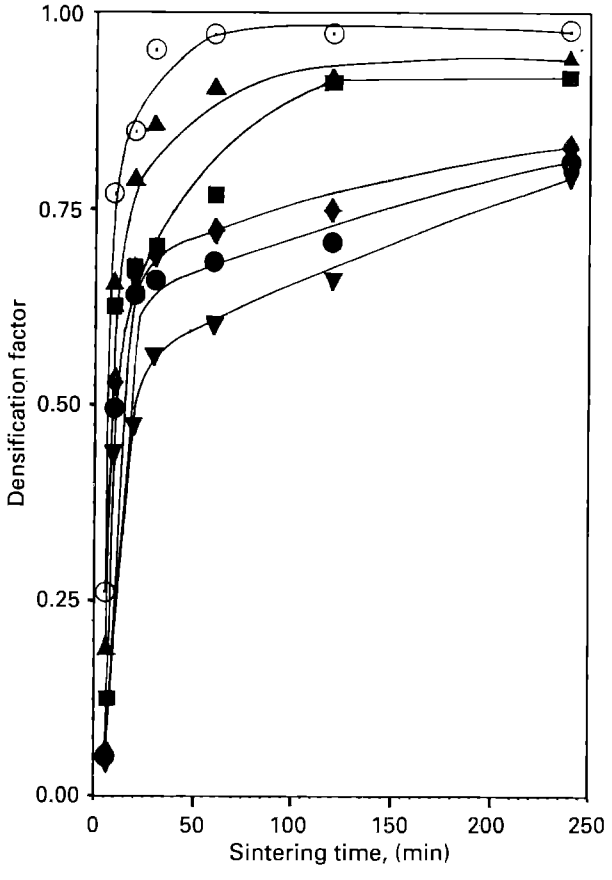

Figure 6 Densification factor against sintering time at 1200 °C: pure HA (○); composites containing 5 (▲), 10 (■), 15 (◆), 20 (●) and 30 (▼) vol % Ag.

3.2. X-ray diffraction and Ca/P ratio

The powder X-ray diffraction pattern of as-received HA (Fig. 7a) did not contain any peak other than

those of HA. However, the peaks were broadened and noise was superimposed on the pattern, possibly due to the presence of amorphous calcium phosphate [37]. The Ca/P ratio in the as-received HA was measured to be 1.61 ± 0.05, which is slightly lower than that (1.67) of perfect HA. But upon sintering in air at 1200 °C for 1 h, the Ca/P ratio of HA increased to 1.70 ± 0.03. Moreover, the peaks in the powder diffraction pattern of sintered HA (Fig. 7b) became sharper and had less noise than those of as-received HA. Sintering at 1200 °C crystallized most of the amorphous phase and thus made the diffraction pattern sharper.

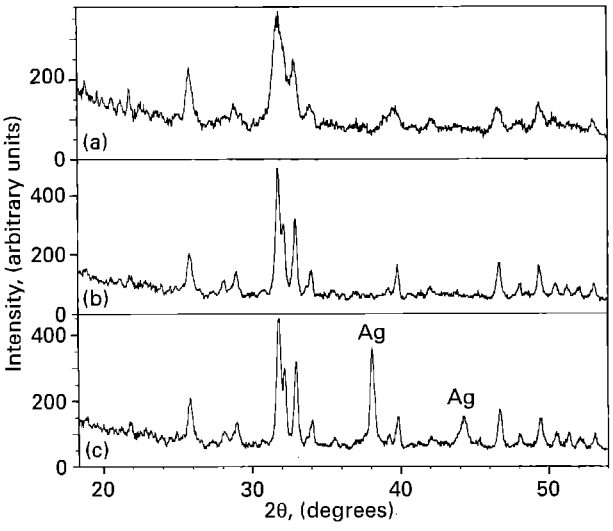

Figure 7 Powder x-ray diffraction patterns: (a) as-received HA; (b) HA sintered in air at 1200 °C for 1 h; (c) HA-10 vol % Ag composite sintered in air at 1200 °C for 1 h.

Fig. 7c shows the powder X-ray diffraction pattern of HA-10 vol % Ag composite sintered in air at 1200 °C for 1 h. The pattern contained only the peaks of HA and Ag. There was no peak due to formation of Ag_3PO_4 [30]. Thus, Ag did not react with HA during sintering at 1200 °C in air. Furthermore, Ca/P ratios of HA-5 vol % Ag and HA-10 vol % Ag composites (prepared by sintering in air at 1200 °C for 1 h) were measured to be 1.73 ± 0.04 and 1.74 ± 0.04, respectively, indicating that the quality of HA in the composites was good.

3.3. Microstructure

Fig. 8a is an optical micrograph showing the microstructure of pure HA compact sintered in air at 1200 °C for 1 h. The intercept grain size of this compact was 1.67 ± 0.07 μm. Fig. 8b shows the microstructure of HA-10 vol % Ag composite sintered in air at 1200 °C for 1 h. The grain size of HA in this composite was 1.42 ± 0.08 μm, which was lower than that of pure HA sintered at identical conditions. Fig. 9 shows the plot of the grain sizes of pure HA and HA-10 vol % Ag composite against time during sintering in air at 1200 °C. In the case of pure HA, the grain size increased rapidly with sintering time, reaching 4.4 ± 0.2 μm at 240 min. On the other hand, the grain size of HA-10 vol % Ag composite increased rapidly at the beginning of sintering, but eventually reached a plateau with a value of 1.7 ± 0.3 μm at 240 min. At all periods of sintering time the grain size of HA-10 vol % Ag composite was lower than the corresponding grain size of pure HA compact. Thus, Ag caused stagnation of grain growth [38] by pinning the grain boundaries.

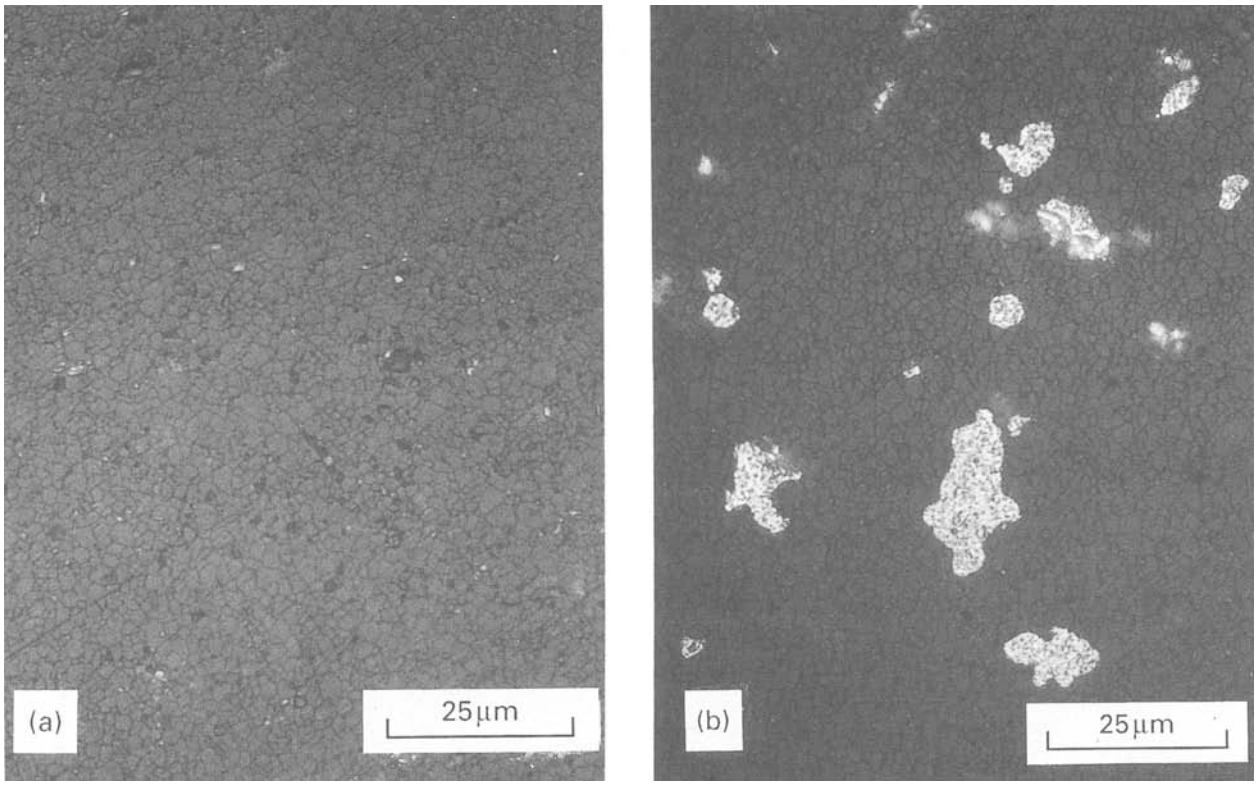

Figure 8 Optical micrographs of polished and etched cross-sections of pure HA (a) and HA-10 vol % Ag composite (b). Both materials were sintered in air at 1200 °C for 1 h. The white portions in (b) are Ag inclusions.

Another interesting observation which can be made from Fig. 8b is that the average size of Ag inclusions in HA-10 vol % Ag composite sintered in air at 1200 °C for 1 h was about 10 μm, while the initial size of Ag particles was 1–3 μm. During sintering at 1200 °C Ag melted, but, due to poor wetting with HA, did not flow in between HA particles. Instead, a few adjacent Ag particles joined together, creating large inclusions in the composite. Even though Ag melted during sintering, HA particles in the composite were bonded together by solid-phase sintering, rather than liquid-phase sintering [39]. The lack of wetting between HA and Ag (due to high interface energy between HA and molten Ag) affected densification (as discussed in Section 3.1) of the composites adversely. To reduce interface energy, the Ag particles tended to join together or escape to the free surface, leaving pores. As a result, the composites with higher Ag contents reached lower relative densities.

The HA grains in contact with Ag inclusions in the composite were larger (Fig. 8b) than the average grain size. This abnormal grain size can be explained by the solution-precipitation process [40], which involved dissolution of HA in molten Ag and then precipitation back, thereby enlarging the HA grains adjacent to Ag inclusions.

Grain growth is an activated process [41] with Arrhenius-type temperature dependence:

$$d = K_0 \exp\left[-\frac{Q}{RT}\right] \quad (5)$$

where d is the average grain size obtained upon sintering for a fixed period of time, T is the sintering temperature, Q is the activation energy, K_0 is a constant and R is the universal gas constant. Fig. 10 shows the plots of logarithm of grain size against the reciprocal of the sintering temperature for pure HA and HA-10 vol % Ag composite obtained upon sintering for 4 h in air. The curve for pure HA had three stages (Fig. 10). At low temperatures (below 1000 °C) the grain size remained small (Table II), and consequently, grain boundary diffusion contributes predominantly to grain growth [42, 43]. At intermediate temperatures where grain sizes were larger (Table II), bulk diffusion contributes to grain growth and, as a result, the curves in Fig. 10 were steep. The activation energy (measured from the slope of the curve in Fig. 10) of grain growth in pure HA in the temperature range 1000–1200 °C was 36 kcal mol^{-1}. Jarcho *et al.* [44] reported a higher value (56 kcal mol^{-1}) of activation energy of grain growth during sintering of their HA compacts. At very high temperatures (> 1200 °C) the slope of the log (grain size) versus $1/T$ curve (Fig. 10) was smaller than that at the intermediate temperature, possibly due to the fact that at high temperatures the diffusion coefficients of the elements in HA change owing to dehydroxylation and decomposition of HA [17]. The log (grain size) versus $1/T$ curve (Fig. 10) for HA-10 vol % Ag composite was similar to that of pure HA, except that the slope remained the same in the temperature range 1100–1250 °C. At every temperature the grain size of

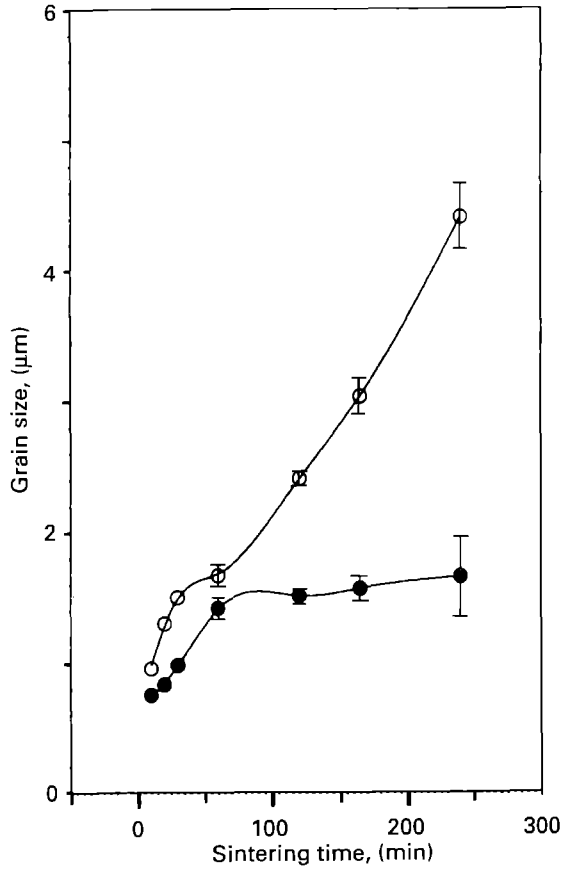

Figure 9 Grain size against time for sintering in air at 1200 °C: (○) pure HA; (●) HA-10 vol % Ag composite.

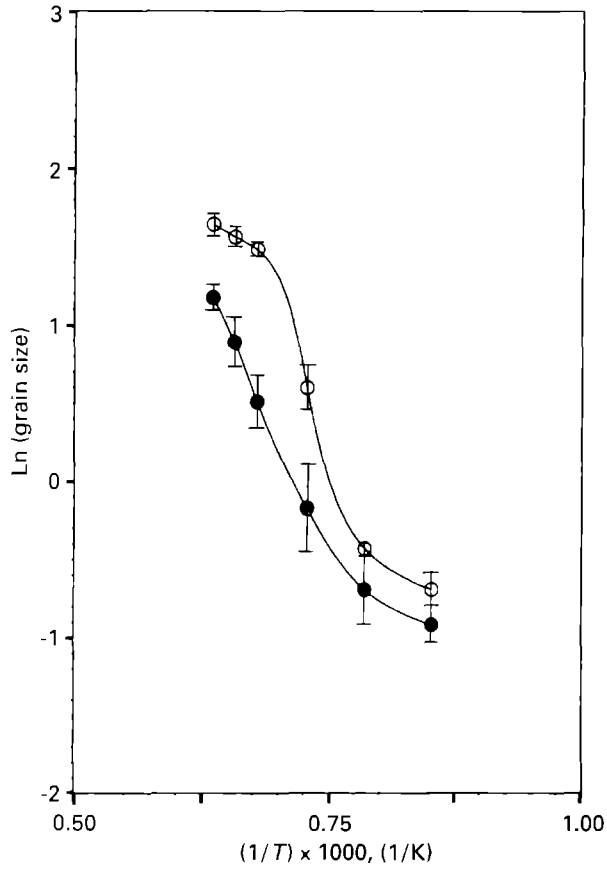

Figure 10 Natural logarithm of grain size against the reciprocal of temperature during sintering in air for 4 h: (○) pure HA; (●) HA-10 vol % Ag composite.

TABLE II Grain size (μm) after sintering at various temperatures for 4 h in air (values are mean ± standard deviation).

Material	Sintering temperature (°C)					
	900	1000	1100	1200	1250	1300
HA	0.5 ± 0.1	0.6 ± 0.1	1.8 ± 0.3	4.4 ± 0.2	4.8 ± 0.3	5.2 ± 0.4
HA-10 vol % Ag	0.4 ± 0.1	0.5 ± 0.1	0.8 ± 0.3	1.7 ± 0.3	2.4 ± 0.4	3.2 ± 0.3

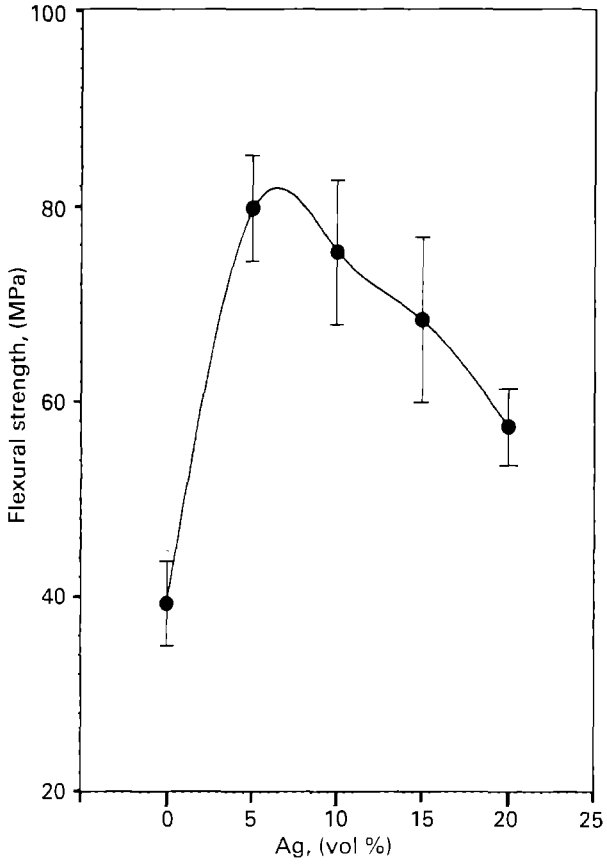

Figure 11 Flexural strength of HA–Ag composites against the volume fraction of Ag. Sintering was in air at 1200 °C for 1 h.

the composite (Table II) was lower than that of pure HA. The activation energy of grain growth during sintering of the composite in the temperature range 1100–1250 °C was 29 kcal mol^{-1}, which was lower than that of pure HA at intermediate temperatures. In the case of the composites the increasing temperature had a role in reducing Zener drag [45] of grain boundaries pinned by Ag.

3.4. Flexural strength

Fig. 11 shows the flexural strength of HA–Ag composites against the volume fraction of Ag. All the composites and pure HA were sintered in air at 1200 °C for 1 h. The addition of Ag increased the flexural strength. The flexural strength of HA-5 vol % Ag composite was 80 ± 5 MPa, compared to a value of 39 ± 4 MPa for pure HA. The flexural strength started to decrease at Ag contents greater than 5 vol %. The flexural strength of HA-10 vol % Ag composite was 75 ± 7 MPa and this is still a significant improvement, considering the fact that the density of the composite was 90 ± 2%, compared to a value of

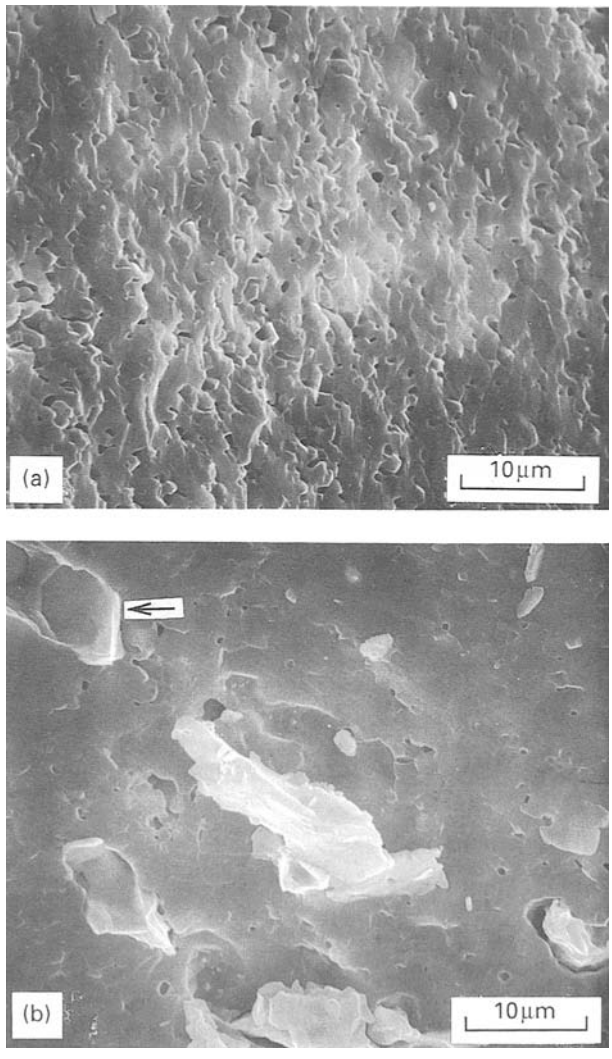

Figure 12 Scanning electron micrographs of the fracture surface: (a) pure HA; (b) HA-10 vol % Ag composite. The white portions in (b) are resolidified Ag inclusions.

98.7 ± 0.4% for pure HA. We showed earlier (Fig. 3) that the relative density of the composite decreased with the increasing Ag content. The porosity deteriorated the flexural strength of the composites at high Ag contents.

Fig. 12a and b show the fracture surface of the bars (broken in four-point bending test) of pure HA and HA-10 vol % Ag composite, respectively. Both materials were sintered in air at 1200 °C for 1 h. The fracture in both pure HA and HA-10 vol % Ag composite were of cleavage type. In the composite the crack also propagated along the interface between HA and Ag, leaving Ag inclusions on the fracture surface (white spots in Fig. 12b) or pulling out Ag inclusions from the fracture surface (indicated by an arrow in Fig. 12b).

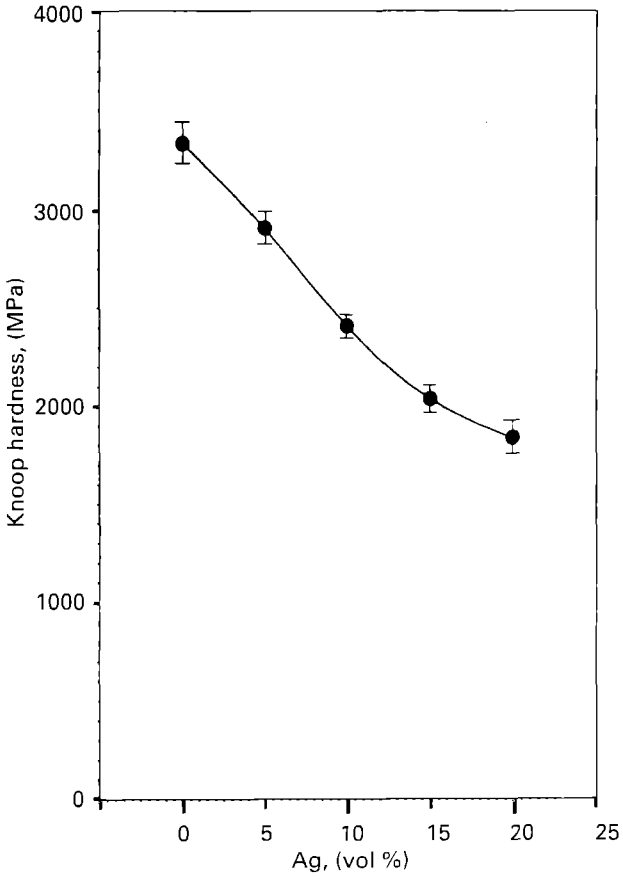

Figure 13 Knoop hardness of HA–Ag composites against the volume fraction of Ag.

No fractured Ag inclusion was observed on the fracture surface of HA–Ag composites. The crack going around Ag inclusions along the HA–Ag interface can produce crack bridging [25], which can increase the flexural strength of HA–Ag composites.

The fracture surfaces in Fig. 12a and b contained micropores (shown as black dots). Pure HA, represented in Fig. 12a, contained 1.3 vol % porosity (density of 98.7 ± 0.4%) distributed uniformly as fine pores of size 0.2–0.5 μm. HA-10 vol % Ag composite, containing 10 vol % porosity, contained pores of size 0.5–1 μm (Fig. 12b). There were bigger pores (1–2 μm) adjacent to Ag inclusions (Fig. 12b), and these pores possibly grew due to shrinkage of molten Ag during solidification.

3.5. Microhardness and indentation cracks

Fig. 13 shows the Knoop hardness (measured under 200 g load) of HA–Ag composites against the volume fraction of Ag. All the composites and pure HA were sintered in air at 1200 °C for 1 h. Indentations were made on the polished surface without any direct hit on Ag inclusions. Each datum point is the average of at least ten measurements. The Knoop hardness decreased with increasing Ag content (Fig. 13). The variation in the hardness with Ag content was exactly similar to that of densification (Fig. 3), indicating that hardness was essentially controlled by the bonding among the particles in the sintered compacts.

Fig. 14 shows an indentation crack generated from a corner of a Vickers indenter in HA-10 vol % Ag composite (sintered in air at 1200 °C for 1 h). The crack started from the upper right side of the micrograph and propagated downward beneath two Ag inclusions which formed bridges [25] in the wake of the crack tip. The crack eventually stopped at the third Ag inclusion. Thus, ductile Ag inclusions hindered the growth of cracks in HA–Ag composites, producing a reinforcing effect in the brittle HA-matrix.

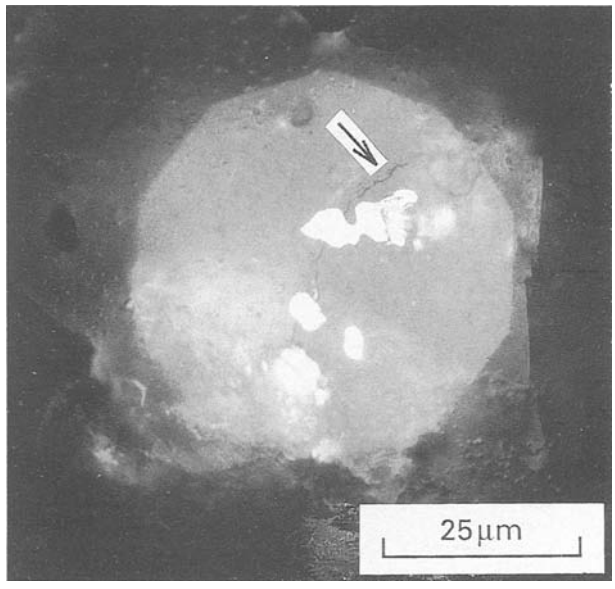

Figure 14 Optical micrograph of an indentation crack (shown by an arrow).

4. Conclusions

HA-matrix Ag composites were prepared successfully by sintering a mixture of HA and Ag powders. A HA-10 vol % Ag composite, prepared by sintering in air at 1200 °C for 1 h, achieved a density of 90 ± 2% of the theoretical density and a flexural strength of 75 ± 7 MPa. Pure HA, sintered under identical conditions, had a density of 98.7 ± 0.4% and a flexural strength of 39 ± 4 MPa. Thus, Ag provided a considerable reinforcement to HA. The powder X-ray diffraction study did not indicate any decomposition of HA or any reaction of HA and Ag at the sintering temperature of 1200 °C. Ag melted during sintering, but, due to poor wettability, did not flow around HA particles. Rather, crack bridging and arrests at isolated Ag inclusions caused the reinforcement of HA-matrix Ag composites.

Acknowledgements

The authors would like to thank Professor George Nancollas of the State University of New York at Buffalo for his kind help in the measurement of the Ca/P ratio in HA.

References

1. J. R. VAN WAZER, "Phosphorous and its compounds", Vol. I and II (Interscience, New York, 1958).
2. J. S. HANKER and B. L. GIAMMARA, *Science* **242** (1988) 885.

3. M. JARCHO, *Clin. Ortho. Rel. Res.* **157** (1981) 259.
4. C. LAVERNIA and J. M. SCHOENUNG, *Ceram. Bull.* **70** (1991) 95.
5. A. S. POSNER, A. PERLOFF and A. D. DIORIO, *Acta Crystallog.* **11** (1958) 308.
6. P. DUCHEYNE and K. DE GROOT, *J. Biomed. Mater. Res.* **15** (1981) 441.
7. R. E. HOLMES, *Plastic Recons. Surg.* **63** (1979) 626.
8. E. A. MONROE, W. VOTAYA, D. B. BASS and J. MCMULLEN, *J. Dent. Res.* **50** (1971) 860.
9. H. DENISSEN, C. MANGANO and G. VENINI, "Hydroxyapatite implants" (Piccin Nuova Libraria, S.P.A., Padua, 1985) p. 19.
10. M. WINTER, P. GRISS, K. DE GROOT, H. TAGAI, G. HEIMKE, H. J. A. V. DIJK and K. SAWAI, *Biomaterials* **2** (1981) 159.
11. R. E. HOLMES and S. M. ROSER, *Int. J. Oral Maxillofac. Surg.* **16** (1987) 718.
12. J. W. FRAME, P. G. J. ROUT and R. M. BROWNE, *ibid.* **18** (1989) 142.
13. C. CHANG, V. J. MATUKAS and J. E. LEMONS, *ibid.* **41** (1983) 729.
14. G. L. DE LANGE, C. DE PUTTER, K. DE GROOT and E. H. BURGER, *J. Dent. Res.* **68** (1989) 509.
15. S.-Y. CHAO and C.-K. POON, *J. Oral Maxillofac. Surg.* **45** (1987) 359.
16. D. G. PAGE and D. LASKIN, *ibid.* **45** (1987) 356.
17. P. E. WANG and T. K. CHAKI, *J. Mater. Sci. Mater. Med.* **4** (1993) 150.
18. J. HANKER, J. RAUSCH, S. LI, W. AMBROSE, C. HOWARD, M. TUCKER, C. LUPTON and B. TERRY, *J. Dent. Res.* **63** (1984) 325.
19. B. BRIDGE, *Brit. J. NDT* **29** (1987) 418.
20. K. ISHIHARA, H. ARAI, N. NAKABAYASHI, S. MORITA and K. FURUYA, *J. Biomed. Mater. Res.* **26** (1992) 937.
21. C. C. P. M. VERHEYEN, J. R. DE WIJN, C. A. VAN BLITTERSWIJK and K. DE GROOT, *ibid.* **26** (1992) 1277.
22. H. JI and P. M. MARQUIS, *Biomaterials* **13** (1992) 744.
23. A. BERTOLUZZA, R. SIMONI, A. TINTI, M. MOROCUTTI, V. OTTANI and A. RUGGERI, *J. Biomed. Mater. Res.* **25** (1991) 23.
24. W. D. KINGERY, H. K. BOWEN and D. R. UHLMANN, "Introduction to ceramics", 2nd Edn (Wiley-Interscience, New York, 1976) p. 573.
25. P. A. MATAGA, *Acta Metall.* **37** (1989) 3349.
26. B. D. FLINN, M. RÜHLE and A. G. EVANS, *ibid.* **37** (1989) 3001.
27. V. D. KRSTIC and M. KOMAC, *Phil. Mag. A* **51** (1985) 191.
28. K. T. VENKATESWARA RAO, W. O. SOBOYEJO and R. O. RITCHIE, *Metall. Trans.* **23A** (1992) 2244.
29. R. ROGIER and F. PERNOT, *J. Mater. Sci.* **26** (1991) 5664.
30. K. HANGST, J. EITENMÜLEER, R. WELTIN and G. PETERS, in "Biomedical materials and devices", edited by J. S. Hanker and B. L. Giammara (Materials Research Society, Pittsburgh, 1987) 269.
31. A. GEE and V. R. DEITZ, *Analytical Chem.* **25** (1953) 1320.
32. J.-H. JEAN and T. K. GUPTA, *J. Mater. Sci.* **27** (1992) 1575.
33. Military Standard, MIL-STD-1942 (MR), "Flexural strength of high performance ceramics at ambient temperature" (Department of the Army, Washington, DC, USA, November 1983).
34. J. E. HILLIARD, *Met. Prog.* **85** (1964) 99.
35. R. M. GERMAN, "Particle packing characteristics" (Metal Powder Industries Federation, Princeton, NJ, 1989).
36. V. N. EREMENKO, YU. V. NAIDICH and I. A. LAVRINENKO, "Liquid-phase sintering" (Consultants Bureau, NY, 1970) p. 34.
37. M. WEINLAENDER, J. BEUMER III, E. B. KENNEY, P. K. MOY and F. ADAR, *J. Mater. Sci. Mater. Med.* **3** (1992) 397.
38. C. H. WÖRNER and P. M. HAZZLEDINE, *JOM* **44** (1992) 16.
39. R. M. GERMAN, "Liquid phase sintering" (Plenum Press, NY, 1985).
40. G. H. S. PRICE, C. J. SMITHELLS and S. V. WILLIAMS, *J. Inst. Met.* **62** (1938) 239.
41. P. FELTHAM and G. J. COPLEY, *Acta Metall.* **6** (1958) 539.
42. G. C. KUCZYNSKI, *ibid.* **4** (1956) 58.
43. R. L. COBLE, *J. Appl. Phys.* **32** (1961) 787.
44. M. JARCHO, C. H. BOLEN, M. B. THOMAS, J. BOBICK, J. F. KAY and R. H. DOREMUS, *J. Mater. Sci.* **11** (1976) 2027.
45. C. S. SMITH, *Trans. AIME* **175** (1948) 15.

Received 19 February and accepted 2 December 1993